arXiv:2608.09537v1 [cs.AI] 10 Aug 2026

VERDI: RETRIEVAL IS NOT TRANSFER FOR CONTINUAL WORLD MODEL OPTIMIZATION

Junyu Wu*, Shiqin Nie*, Youyi Kou, Baohua Yin, Guocai Yao, Qingyu Chen, Jingheng Ma, Shiji Zhou, Hongyong Song, Mingchen Zhuge, Sen Cui‡,†, Changshui Zhang†

* *Equal contribution,* ‡ *Project leader,* † *Corresponding author*

Project page: `https://verdiwm-anno.github.io/`

ABSTRACT

Foundation world models have made remarkable progress in planning, simulation, and embodied intelligence. However, optimizing a pretrained world model toward a user-specified objective remains difficult: each campaign typically rediscovers optimization strategies from scratch, and the resulting knowledge rarely transfers to the next model. Existing research agents automate the optimization loop but treat successful strategies as directly reusable recipes, without principled safeguards for when transfer is appropriate. We argue instead that *retrieval is not transfer*: a strategy validated on one model is at best an optimization *hypothesis* for another, and becomes transferable knowledge only after target-side experimental validation. Guided by this principle, we propose VERDI , a continual framework for evidence-licensed world model optimization. VERDI characterizes each world model through shared inference-time probes to construct an Optimization Fingerprint, retrieves relevant prior experience as ranked hypotheses, and validates every candidate under a frozen target-side verifier before admitting it as reusable evidence; contradictions among nearby fingerprints further trigger probe evolution, continually refining the diagnostic representation itself. Experiments on Ctrl-World, the Cosmos family, and RoboCoin show that VERDI reduces search cost by 68%, GPU cost by 69%, and negative transfer from 0.34 to 0.06, while predicting transfer outcomes with 83% sign accuracy.[1]

1 INTRODUCTION

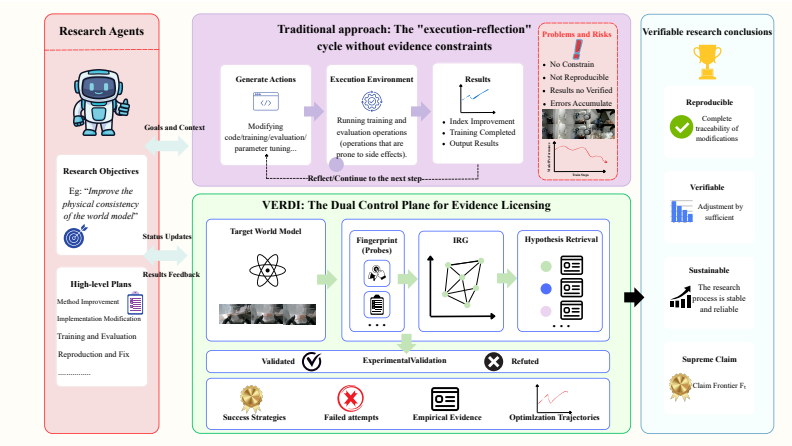


Figure 1: Comparison between Verdi and other agents.

Foundation world models have become a fundamental component of embodied intelligence, enabling planning, policy learning, synthetic data generation, and simulation through predictive modeling

[1]E-mail: `zcs@mail.tsinghua.edu.cn`, `cuis@mail.tsinghua.edu.cn`

of future observations (Ha and Schmidhuber, 2018; Hafner et al., 2020; 2025); as foundation models continue to diversify in architecture, scale, and capability (NVIDIA et al., 2025; Guo et al., 2025), improving pretrained world models toward user-specified objectives has become increasingly important. Recent advances in autonomous research agents further demonstrate that much of the optimization pipeline—including experiment generation, implementation, execution, and evaluation—can be automated, making world model optimization an increasingly autonomous process in practice (Lu et al., 2024; Huang et al., 2024; Chan et al., 2025).

Despite this progress, world model optimization remains fundamentally non-cumulative: each optimization campaign typically starts from a pretrained world model, explores numerous optimization strategies, validates those that improve the target objective, and terminates once the objective is achieved. While this process continuously produces valuable optimization knowledge, including successful optimization strategies, failed attempts, empirical evidence, and optimization trajectories, such knowledge is rarely reused beyond the current model. Consequently, every newly developed world model largely repeats the same optimization process from scratch, rediscovering optimization knowledge that has already been obtained for previous models. This lack of knowledge accumulation is becoming an increasingly important bottleneck as the number and diversity of world models continue to grow across the field as their diversity increases.

A key challenge is that optimization knowledge is inherently model-dependent, yet existing systems lack a principled way to relate heterogeneous world models from the perspective of optimization. Similar architectures do not necessarily exhibit similar optimization behaviors, while architecturally different world models may benefit from remarkably similar optimization strategies. Therefore, effective knowledge transfer requires comparing world models according to their optimization-relevant characteristics rather than their implementation details. We hypothesize that these characteristics can be actively measured through a shared set of inference-time probes. Based on the resulting probe responses, we construct an *Optimization Fingerprint* for each world model and define an *Interventional Repair Geometry* (IRG) over these fingerprints, providing a principled basis for measuring optimization similarity and retrieving potentially transferable optimization knowledge.

Building on this insight, we propose VERDI, a framework for continual and transferable world model optimization. Given a new model and objective, VERDI characterizes the model with shared probes and computes its Optimization Fingerprint. It then compares the fingerprint with prior models through IRG to retrieve relevant experience as optimization hypotheses rather than direct transfers. VERDI designs and executes experiments, validates candidate strategies, and incorporates verified evidence into an evolving *WMOM*. As campaigns accumulate, both optimization knowledge and the probing mechanism evolve, progressively improving transfer across heterogeneous world models and campaign settings.

We evaluate VERDI on representative world model families under diverse optimization objectives, including backbone optimization, cross-model optimization transfer, and adaptation to previously unseen optimization goals. Experimental results demonstrate that VERDI consistently retrieves more relevant optimization knowledge, improves optimization efficiency, and enables reliable optimization transfer across heterogeneous world models. More broadly, our results suggest a new paradigm in which world model optimization evolves from isolated optimization campaigns into a continually improving optimization knowledge system.

Our main contributions are summarized as follows:

- **We reveal the phenomenon that direct retrieval is not transfer.** We introduce a principled representation and comparison mechanism that measures optimization similarity through shared inference-time probes, providing the foundation for transferable optimization knowledge across future campaigns.
- **We propose a continual optimization methodology for world models.** We formulate world model optimization as a continual optimization-knowledge accumulation process, enabling optimization experience to be systematically reused across heterogeneous world models. Each repair is represented as a paired, multi-coordinate effect rather than an absolute score, making trade-offs explicit before transfer decisions.
- **Verdi.** We develop and release an autonomous framework that retrieves, validates, and continually accumulates world model optimization knowledge, enabling efficient and reliable optimization transfer across heterogeneous world model families including Ctrl-World, Cosmos, and RoboCoin.

2 RELATED WORK

World-model evaluation. Recent embodied world-model benchmarks move evaluation from perceptual fidelity toward functional utility: EWMBench (Yue et al., 2025) assesses scene, motion, and semantic quality; WorldArena (Shang et al., 2026a) unifies 16 video metrics with embodied tasks (data engine, policy evaluation, action planning) and reports a persistent gap between visual quality and downstream utility; WorldArena 2.0 (Shang et al., 2026b) further adds visuotactile modalities and interactive policy training. Complementarily, large-scale studies such as GigaWorld (GigaAI, 2025) expose correlation structure among metric families. These works characterize what is broken and which metrics trade off; we build our validity gates and candidate generation on such structure and answer the complementary question: which repair will fix a given model, and can that knowledge move to the next one in a future campaign.

World-model improvement. Progress is driven by per-model effort: controllable manipulation world models (Guo et al., 2025; Zhu et al., 2025a), foundation platforms (NVIDIA et al., 2025), interactive environments (Google DeepMind, 2025), and reward-model alignment for downstream policy success (Han and Yilmaz, 2026). Each improves one backbone at a time; VERDI instead treats improvement itself as the learning problem, accumulating verified, context-annotated repairs that transfer across models under matched support.

Self-improving and research agents. Recent systems let agents run research, modify models, or implement code autonomously: SWE-agent (Yang et al., 2024), Agent Laboratory (Schmidgall et al., 2025), The AI Scientist (Lu et al., 2024), Agent Laboratory (Schmidgall et al., 2025), SWE-agent (Yang et al., 2024), AlphaEvolve (Novikov et al., 2025), the Darwin-Gödel machine (Zhang et al., 2025), Karpathy's autoresearch loop (Karpathy, 2026), pipeline frameworks such as AutoResearchClaw (AutoResearchClaw Team, 2025), and agentic robotics systems that unify collection, learning, and execution such as RoboClaw (Li et al., 2026). Benchmarks such as CORE-Bench and PaperBench also expose reproducibility and faithful-replication bottlenecks (Siegel et al., 2024; Starace et al., 2025), while follow-up analyses caution that implementation capability can limit apparent scientific autonomy (Beel et al., 2025; Zhu et al., 2025b). Benchmarks such as CORE-Bench and PaperBench also expose reproducibility and faithful-replication bottlenecks (Siegel et al., 2024; Starace et al., 2025), while follow-up analyses caution that implementation capability can limit apparent scientific autonomy (Beel et al., 2025; Zhu et al., 2025b). These works demonstrate that agents can propose, run, and iterate—but they reuse experience opportunistically, with no mechanism for deciding when experience is safe to move across models, and their evaluation can drift together with the agent. Closest to us is ENPIRE (Xie et al., 2026), which closes a real-robot loop in which coding agents reset scenes, verify outcomes, and iteratively improve manipulation policies. ENPIRE improves policies within a fixed task; VERDI improves world models and, crucially, decides whether verified repair knowledge may move to a different model: transfer is licensed by a certificate with explicit abstention, the verifier is frozen within a campaign, and failed transfers feed back as counterexamples that refine the representation itself rather than merely extending the candidate pool itself.

3 METHOD

Overview. Verdi formulates continual world model optimization as a four-stage process: *Characterize* $\rightarrow$ *Retrieve* $\rightarrow$ *Validate* $\rightarrow$ *Accumulate*. Given a target world model and a user-specified optimization objective, Verdi first characterizes the model through a shared library of inference-time probes, producing an Optimization Fingerprint that captures optimization-relevant behavior. The fingerprint is then related to previously optimized world models through the Interventional Repair Geometry (IRG), allowing the system to retrieve candidate Optimization Skills as *optimization hypotheses*. Rather than assuming retrieved knowledge is transferable, Verdi validates every hypothesis through target-side optimization experiments under a frozen verifier. Only experimentally settled evidence, including confirmed positive, null, harmful, and interaction outcomes, is incorporated into the WMOM. Consequently, optimization similarity serves only to prioritize and guide experiments, while transferable optimization knowledge is established exclusively through experimental validation and continually accumulated for future optimization. Figure 2 summarizes this continual evidence loop.

Problem setting. Let a world model M_θ produce a rollout

$$\hat{\tau}_{1:H} = \mathrm{Rollout}(M_\theta; \mathbf{c}, \mathbf{u}), \tag{1}$$

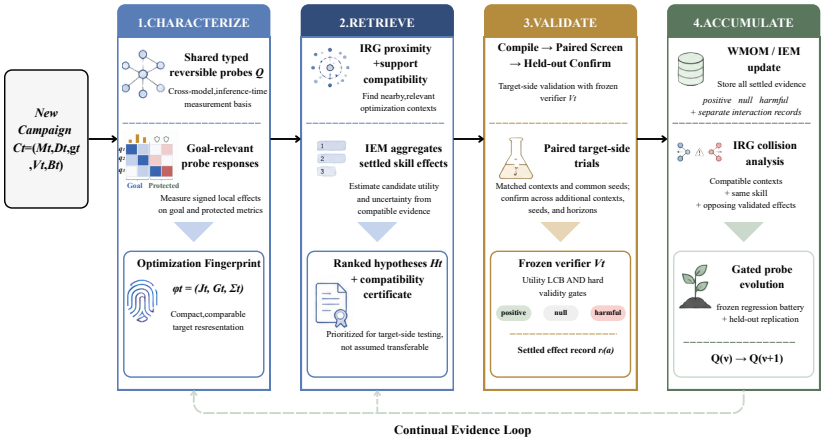


Figure 2: **Continual evidence loop of Verdi.** The framework (1) characterizes a new campaign with typed probes and an Optimization Fingerprint; (2) retrieves ranked hypotheses using IRG proximity and support compatibility; (3) validates each hypothesis through paired target-side screens and held-out confirmation under a frozen verifier; and (4) accumulates settled positive, null, harmful, and interaction outcomes in WMOM/IEM. Opposing validated effects trigger IRG collision analysis and gated probe evolution, closing the evidence loop.

where $\mathbf{c}$ denotes observations, language, or task context and $\mathbf{u}$ denotes optional actions or controls. This interface covers action-conditioned world models (ACWMs), which predict future observations, and world-action models (WAMs), which may additionally predict actions, progress, success, or safety events. An optimization campaign $\mathcal{C}_x = (M_x, \mathcal{D}_x, \mathcal{G}_x, V_x, B_x)$ fixes a target model, permitted data, user goal, frozen verifier, and nominal resource allowance. The goal defines a primary utility $U_{\mathcal{G}_x}$, validity constraints $g_{x,j}$, and improvement threshold $\tau_{\mathcal{G}_x}$. An Optimization Skill a is an executable procedure applied to M_x within this budget; its settled effect record $r_x(a)$ contains the paired utility change $\Delta U_x(a)$ and validity outcomes. We use t for the target campaign and s for a retrieved source campaign. A trial is one candidate attempt admitted to the search loop; screening, compilation rejection, and confirmation are recorded as subevents, while rollout seeds do not create additional trials. A trial is positive only when its paired utility improvement exceeds the threshold and every validity constraint passes for acceptance.

Differential repair contract. A differential repair is a typed intervention whose claim is defined by a paired change vector rather than by an absolute score. Let $\mathbf{y}_x(a)$ collect the target utility and protected outcomes after applying skill a, and let $\mathbf{y}_x(0)$ denote the matched control under the same contexts, seeds, and verifier. We define

$$\Delta\mathbf{y}_x(a) = \mathbf{y}_x(a) - \mathbf{y}_x(0), \tag{2}$$

The first coordinate is $\Delta U_x(a)$; protected coordinates are represented as violations $v_{x,j}$, for which $v_{x,j} \leq 0$ passes. A repair is accepted only when $\Delta U_x(a) > \tau_{\mathcal{G}_x}$ and all protected constraints pass. Thus, a gain on one coordinate cannot cancel a violation on another. The same differential signature is used to rank source hypotheses and to validate them on the target; differential refers to the paired intervention effect, not merely to a difference between checkpoints or losses. The resulting online decision and memory-update loop is detailed in Figure 3.

3.1 Characterizing World Models

Inference-time Characterization. Architecture labels and parameter counts are poor proxies for whether the same optimization will work on two world models. Verdi instead measures how each model responds to a shared library of typed, inference-only probes. A probe $q \in \mathcal{Q}$ applies a reversible semantic perturbation with dose α, such as modifying action magnitude, context retention, first-frame anchoring, or sampler noise. It changes neither model parameters nor the optimization objective. Backbone-specific adapters may implement a probe through different hooks, but must

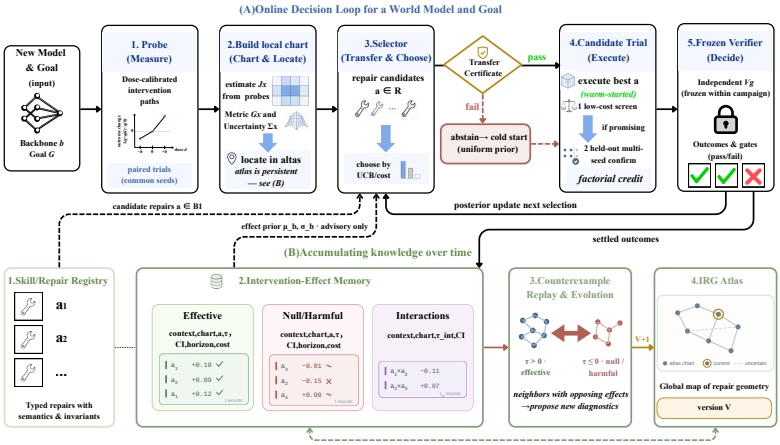


Figure 3: **Detailed online decision and memory-update loop. (A)** Verdi characterizes a target model with shared inference-time probes, relates its Optimization Fingerprint to prior campaigns through the Interventional Repair Geometry (IRG), and retrieves Optimization Skills as hypotheses. Each hypothesis is compiled and tested on the target under a frozen verifier; retrieval never directly changes the model or writes a knowledge claim. **(B)** Confirmed positive, null, harmful, and interaction outcomes update the WMOM. Contradictory outcomes among nearby fingerprints expose missing diagnostic distinctions and drive held-out probe evolution across campaigns.

satisfy the same behavioral contract. We write $M_x^{q,\alpha}$ only as shorthand for the same fixed-parameter model M_x evaluated under the inference intervention T_q^α; it does not denote an updated model.

Let $z(M;\xi,\omega) \in \mathbb{R}^K$ collect diagnostic and validity outcomes for evaluation context ξ and inference seed ω. Matched seeds and contexts for a control and a probed rollout yield the local response

$$J_x[k,q] = \mathbb{E}_{\xi,\omega}\left[\frac{z_k(M_x^{q,\alpha};\xi,\omega) - z_k(M_x;\xi,\omega)}{\alpha}\right], \tag{3}$$

and its bootstrap uncertainty Σ_x. Paired responses suppress rollout-level variance and expose behavioral directions that are relevant to optimization but invisible from implementation details alone.

Optimization Fingerprints. For campaign x, VERDI estimates the response Jacobian J_x, its bootstrap covariance Σ_x, and the uncertainty-aware metric

$$G_x = J_x^\top W_x J_x, \tag{4}$$

where W_x standardizes outcome scale and discounts uncertain coordinates. The Optimization Fingerprint

$$\phi_x = \left(J_x, G_x, \Sigma_x\right) \tag{5}$$

summarizes how the model responds, which probe directions are behaviorally distinguishable, and how precisely those responses were measured. Here, ϕ_t is the Optimization Fingerprint of the target campaign $\mathcal{C}_t$, obtained by applying the shared probe library to its target model under its goal and evaluation support; ϕ_s is the corresponding fingerprint of a historical source campaign.

3.2 RETRIEVING OPTIMIZATION KNOWLEDGE

Relating World Models through IRG. IRG defines optimization similarity through shared responses to controlled inference interventions rather than implementation similarity. It asks not whether two world models have similar architectures, parameters, or training histories, but whether the same semantic probes induce comparable changes in optimization-relevant behavior. Typed probe identities and standardized outcomes provide these common coordinates even when backbones have different internals. IRG then compares campaigns using an uncertainty-weighted distance between their fingerprints, augmented by support mismatch. For a goal $\mathcal{G}$, outcome weights select the relevant slice of this geometry, so the same probe bank can support different optimization objectives without being rebuilt for each metric or support condition.

Memory as Experimental Evidence. We use WMOM for the versioned, system-level archive of settled optimization campaigns, receipts, and source–target transfer metadata. Its Intervention-Effect Memory (IEM) is the structured record layer within WMOM. For each settled skill $a = (h, \psi, d, s, p, \iota)$, it stores the source fingerprint, goal, data support, effect vector $r_x(a)$, confidence interval, skill version, cost, and artifact lineage. Here h is the required hook type, ψ the transformation, d the semantic dose, s the schedule, p the preconditions, and ι the invariants. It retains successful skills, null or harmful trials, observed Skill Interactions, and source–target transfer relations. The frozen LOBO archive M_k^{full} is a snapshot of WMOM; retrieval reads its IEM records together with the corresponding IRG and registry metadata. Thus, it answers a specific question: what happened when a particular optimization was experimentally executed for models with similar responses under comparable support contexts?

Optimization Hypothesis Retrieval. For target ϕ_t and skill a, Verdi aggregates compatible source effects using IRG proximity, source evidence quality $\rho_s(a)$, and context overlap κ_{ts}:

$$\widehat{\Delta U}_t(a) = \frac{\sum_{s \in \mathcal{N}_t(a)} w_{ts}(a)\, r_s^U(a)}{\sum_{s \in \mathcal{N}_t(a)} w_{ts}(a)}, \qquad w_{ts}(a) \propto \frac{\rho_s(a)\kappa_{ts}}{\epsilon + \text{dist}_{\text{IRG}}(\phi_t, \phi_s)}. \tag{6}$$

The resulting ranked set $\mathcal{H}_t$ consists of optimization hypotheses, not transferable facts.

3.3 Validating Optimization Transfer

Retrieval is not Transfer. The central safeguard in Verdi is that no retrieved skill becomes knowledge merely because it is close in IRG. A compatibility certificate only decides whether a skill may receive a transfer-prioritized trial. It never certifies the target-side effect and never updates the memory or its evidence in the archive as an accepted record.

Compatibility Check. Before a transfer-prioritized trial, the compatibility certificate checks whether the target can faithfully compile the required mechanism, whether source and target have sufficient support overlap and aligned probe responses, whether enough effective source evidence is available, and whether nearby evidence predicts a consistent effect sign. We write every protected constraint as a violation v_j: $v_j \le 0$ passes and $v_j > 0$ fails. Formally, the transfer-prioritization certificate is

$$\begin{aligned} C_t(a) = \mathbb{I}[\mathsf{compile} = 1]\mathbb{I}[\mathsf{overlap} \ge \rho_{min}]\mathbb{I}[N_{\text{eff}} \ge n_{\min}] \\ \cdot \mathbb{I}[e_{\text{align}} \le \epsilon_{\text{align}}]\mathbb{I}[\mathsf{sign_agree} \ge \gamma]\mathbb{I}[L_a(\phi_t) > \delta_{\mathcal{G}_t}] \\ \cdot \prod_j \mathbb{I}[\widehat{v}_{t,j}(a) \le 0], \end{aligned} \tag{7}$$

where $L_a(\phi_t)$ is the calibrated one-sided lower bound on the target effect and every indicator is binary. The six certificate terms correspond one-to-one to the six failure modes: compilation failure, insufficient support overlap, insufficient evidence, response misalignment, sign disagreement, and insufficient gain over cold start. The certificate prioritizes an experiment but never accepts a target-side effect as valid under the target-side verifier.

Target-side Experimental Validation. Every candidate is compiled against the target backbone and tested under the campaign's frozen verifier. Verdi first uses paired, low-cost screens to eliminate implausible candidates, then confirms promoted candidates on held-out contexts with increasing rollout horizons, optimization steps, and random seeds. A trial becomes a settled result only if its paired utility improvement has a positive lower confidence bound above $\tau_{\mathcal{G}_t}$ and all validity gates pass. If compilation, compatibility, or validation fails, the skill may still be explored as a local cold-start candidate, but historical evidence supplies no claim of transferability.

3.4 Continual Knowledge Accumulation

Updating WMOM and IEM. After validation, Verdi writes the measured effect $r_t(a)$, uncertainty, support conditions, verifier result, cost, and artifact lineage to the World Model Optimization Memory. Positive outcomes promote reusable skills; confirmed null and harmful outcomes define where a skill should not transfer. When skills are evaluated jointly, their measured interaction is stored as a separate evidence record rather than inferred from individual effects. Likewise, every source–target evaluation adds a Transfer Relation that sharpens the conditions under which retrieved evidence is reliable for future retrieval.

IRG Collision Discovery. An IRG collision occurs when two campaigns are close in the current geometry, have comparable data and context support, and yield incompatible validated effects for the same Optimization Skill. Such a collision is not merely a failed transfer: it is counterevidence that the current probe basis omits a transfer-relevant distinction. Formally, for a skill a, a supported pair (x, y) is a collision when

$$\mathrm{dist}_{\mathrm{IRG}}(\phi_x, \phi_y) \le \epsilon_{\mathrm{IRG}}, \qquad \mathrm{LCB}\big(-r_x^U(a) r_y^U(a)\big) > 0. \tag{8}$$

By contrast, repeated failure without a nearby source effect indicates a missing or unsuitable skill rather than an unsuitable geometry for that campaign.

Probe Evolution. Each discovered collision creates a probe-evolution work order containing the affected contexts, conflicting effects, and admissible hook types. Verdi proposes additional probes from unused diagnostics, parameterized variants, or mechanism-specific tests. Given a candidate probe q, it selects

$$q^* = \arg\max_{q \in \mathcal{Q}_{\mathrm{cand}}} \frac{\mathrm{Regret}(\mathcal{Q}) - \mathrm{Regret}(\mathcal{Q} \cup \{q\})}{\mathrm{Cost}(q)}, \tag{9}$$

subject to a frozen regression battery and a minimum information-gain threshold. A probe enters the next basis version only when its benefit replicates on held-out campaigns. The resulting loop continually expands what the system knows, where it knows it, and how reliably it can reuse that knowledge.

4 Experiments

We evaluate Verdi as a diagnosis–repair loop rather than as a single model modification. The experiments ask three questions: (i) can the loop find failure-specific repairs under a frozen evaluator, (ii) can transfer counterexamples improve the diagnostic representation, and (iii) can repair experience accelerate a held-out backbone without importing harmful changes?

4.1 Experimental Protocol

Protocol. Before each campaign, we freeze the target checkpoint, data split, evaluation contexts and seeds, metric directions and weights, validity gates, candidate primitive pool, and nominal verification allowance. Baseline and repair arms share the same initialization, data, nominal optimization allowance, and evaluator. The original observation interface, tokenizer or VAE, decoder, and renderer remain unchanged unless the selected typed repair explicitly declares that component as its intervention target. Every executed change is recorded by a runtime receipt, preventing an implementation from silently deviating from its declared repair.

For cost accounting, we distinguish the nominal allowance B_{nom}, measured training compute C_{train}, candidate-search cost C_{search}, cost to the first strict-gate positive $C_{\mathrm{first}+}$, and overhead $C_{\mathrm{overhead}} = C_{\mathrm{fingerprint}} + C_{\mathrm{screen}} + C_{\mathrm{confirm}}$. The nominal allowance is matched across arms but is not a hard censoring boundary unless stated explicitly; any overrun remains visible.

Settings and metrics. Metrics are instantiated by the campaign goal rather than imposed as one universal scalar benchmark. ACWM-Phys is our controlled development suite and contains eight environments covering rigid contact, articulated motion, deformable memory, granular and fluid transport, and target-conditioned control. We retain its original data split and evaluator. Its goal combines PSNR, SSIM, negative MSE, and negative masked MSE into a signed utility while retaining every coordinate as a protected outcome. Full-backbone studies add the applicable perceptual, WorldArena-style, rollout-stability, and action-following diagnostics. For world-action settings, task or action quality is evaluated separately from video quality, with a no-action control when action dependence is part of the claim. Verdi retains the complete signed effect vector rather than averaging protected-coordinate regressions into a favorable scalar. Environment-specific rollout horizons are declared before evaluation; averages across environments use only shared horizons.

Progressive verification. All baseline–repair comparisons use paired contexts, seeds, initialization, data, and matched training schedules; measured costs are reported by component. A candidate first passes a low-cost 512-step screen, which determines search order but cannot establish a confirmed claim. Promoted candidates are evaluated with the official 50-step evaluator and, where applicable, a longer checkpoint or multi-seed confirmation. Every result is accompanied by a runtime receipt, checkpoint identity, and evaluator configuration. A result is retained only when its preregistered

Table 1: **Concrete failure-specific repairs across world models.** Verdi selects different executable repairs for distinct diagnosed failures. Arrows report changes from the matched backbone; validity boundaries retain protected regressions rather than averaging them away. These rows are within-backbone case studies rather than held-out transfer results.

Backbone	**Selected repair**	**Matched improvement**	**Recorded boundary**
Ctrl-World (Guo et al., 2025)	latent-motion prior	smoothness $68.75 \rightarrow 81.53$; LPIPS $.1528 \rightarrow .1432$	dynamic degree $45.32 \rightarrow 43.78$
Cosmos-Predict 2 (NVIDIA et al., 2025)	REP / DINOv2 (Oquab et al., 2024) guidance	depth $95.35 \rightarrow 97.05$; smoothness $78.93 \rightarrow 81.31$	background consistency $85.35 \rightarrow 82.73$

Table 2: **Ctrl-World on WorldArena.** Baseline and VerdiWM use matched data and training schedules; arrows indicate the preferred direction.

Metric	Ctrl-World	VerdiWM
Semantic Alignment ↑	90.70	**91.30**
Depth Accuracy ↑	93.28	**96.16**
Aesthetic Quality ↑	32.75	**36.12**
Background Consistency ↑	**86.37**	85.11
Dynamic Degree ↑	**45.32**	43.78
Flow Score ↑	26.54	**30.35**
Motion Smoothness ↑	68.75	**81.53**
Subject Consistency ↑	**84.31**	83.35

confirmation and validity gates pass; otherwise the claim is narrowed or rejected. We therefore distinguish a formal positive from a single-checkpoint pass and from a metric-positive result with an open event-validity check. Detailed budgets, thresholds, seeds, and evaluator contracts are retained with the supplementary experiment artifacts.

4.2 Failure-Specific Repair on ACWM-Phys

We first disable cross-backbone transfer and let Verdi diagnose each target from paired-probe responses, retrieve compatible primitives, and verify the selected candidate under the same frozen gate. The resulting repair choices differ across failure families, testing the premise that a single globally preferred primitive is inadequate. The matched-budget selection-source ablation is reported later in Table 14, where the target backbone is held out.

The selected repairs are mechanism-specific. Guidance scheduling is selected for the two cube/contact environments, self-forcing is selected for articulated motion, and next-forcing or a checkpoint-scale transform is selected for deformable, granular, fluid, and target-conditioned cases. The largest current metric changes occur for robot_arm ($+1.08$ dB PSNR), cloth_move ($+0.94$ dB), pour_water ($+0.85$ dB), and push_sand ($+0.64$ dB). The supplementary material retains the complete per-environment PSNR, SSIM, and masked-MSE deltas together with their evidence status; these numbers do not imply that all environments have the same confirmation strength.

4.3 Concrete Repair Slices Beyond ACWM-Phys

ACWM-Phys supplies a controlled matrix; full world-model codebases test whether a diagnosis can be compiled into an executable intervention. We therefore retain matched slices from the preliminary backbone-specific studies. These studies test within-backbone repair and are kept conceptually separate from the held-out transfer experiment in Section 4.5: they establish that the compiler can turn a diagnosis into a concrete intervention, not that the intervention transfers without target-side verification. Figure 13 provides a qualitative example.

oindent**WorldArena validation.** To connect the repair to downstream world-model utility, we report the matched Ctrl-World comparison on WorldArena alongside the qualitative rollout. The repair improves semantic alignment, depth, aesthetic quality, flow, and motion smoothness, while the protected regressions remain visible.

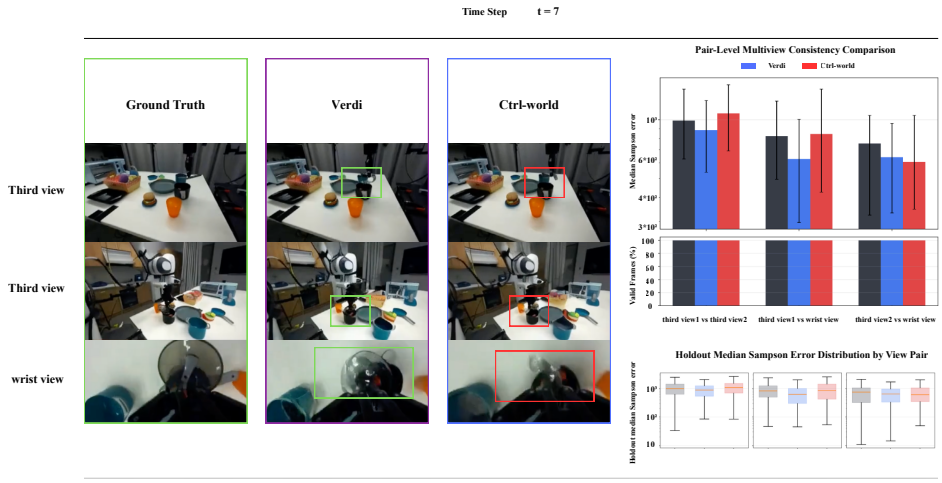


Figure 4: **Visual comparison for the Ctrl-World repair.** Three camera views on the open-lid task show improved consistency in two views, with the third-person view 2 and wrist view retaining the protected regressions recorded in Table 2.

Table 3: **Atlas-evolution policies on nested replay.** Regret is measured against the best admissible repair on held-out domains. Lower is better for regret and calibration error.

Atlas policy	Regret ↓	Calib. error ↓	Probes
Fixed canonical frame	0.29	0.14	4
Free growth	0.31	0.19	14
Collision-driven + regret gate	**0.21**	**0.08**	**7**

The examples also expose why Verdi stores an effect vector rather than a single score. The Ctrl-World repair improves motion smoothness while reducing dynamic degree; the Cosmos-Predict repair improves depth and smoothness while reducing background consistency. Such protected-coordinate regressions form the boundary annotations used by retrieval and certification instead of being hidden by an averaged score. Complete Ctrl-World metrics and multi-view analysis, the Cosmos-Predict 2 and Cosmos3 cases, and the action-quality and dataset-adaptation studies are retained in the original supplementary material for reference.

4.4 Counterexample-Driven Probe Evolution

The second experiment tests whether the diagnostic basis can improve for a reason that is tied to downstream repair selection. The initial *action-dimension anisotropy* probe is local in five of eight environments. A counterexample on cloth move has locality residual 3.88, which triggers a typed proposal for the *action-embedding temporal mix* probe. The successor reduces that residual to 0.0196 on cloth move. It is not globally substituted: on reacher the successor residual is 0.7032, so the conditional library keeps the initial chart there. The resulting local-chart coverage increases from 5/8 to 6/8 (Figure 14) on held-out contexts.

This is evidence for conditional atlas expansion, not evidence of improved world-model quality by itself. The frozen-selector replay currently remains fail-closed for the evolved work orders; accordingly, we do not report an unsupported gain in repair accuracy or regret. The complete locality table and selector control are included in the appendix.

To test whether atlas growth improves repair selection rather than merely adding probe dimensions, we compare the fixed canonical frame, ungated growth, and collision-driven growth in a nested held-out replay. Ungated growth more than triples the frame size without reducing regret, whereas collision-driven growth admits only three additional directions and improves both held-out selection regret and calibration (Table 3) on held-out replay settings.

Table 4: **Held-out cross-backbone transfer.** Lower is better. All policies use the same target evaluator, primitive pool, and nominal allowance; the GPU-h column reports measured $C_{\mathrm{first}+}$.

Transfer mode	Trials to positive ↓	$C_{\mathrm{first}+}$ (GPU-h) ↓	Neg. transfer ↓
Cold start (archive cleared)	11.2	312	–
Unconditional reuse	4.1	118	0.34
Certified reuse (Verdi)	**3.6**	**96**	**0.06**

4.5 Cross-Backbone Selection and Selective Transfer

We isolate repair selection with the executor, registry, nominal allowance, and verifier fixed. The complete intervention fingerprint reaches 0.83 sign agreement, 3.6 trials to positive, 0.06 negative transfer, and 0.03 protected violation; detailed selector controls are reported in Appendix B.9.

We then test held-out transfer. In leave-one-backbone-out (LOBO), each fold freezes a target-independent archive M_k^{full} containing shared prior knowledge and eligible pre-target source campaigns. Target records, calibration data, tuning decisions, and post-evaluation updates are excluded. The two named source backbones are representative, not exhaustive. Cold start sets $M_k^{\mathrm{empty}} = \varnothing$ only for the archive ablation; all other ablations use M_k^{full}. Certified reuse adds fingerprint matching, typed compilation, support/alignment checks, and abstention. All modes use the same primitive pool and nominal allowance; measured $C_{\mathrm{first}+}$ is reported.

The primary outcomes are trials and measured $C_{\mathrm{first}+}$ to the first strict-gate positive, with negative-transfer rate; Table 4 aggregates the rotated held-out folds with fresh target IDs and frozen evaluators before any target update or later archive change.

Certified reuse matches unconditional speed while reducing negative transfer from 0.34 to 0.06; the certificate therefore licenses reuse without promoting harmful or unsupported experience. Fingerprint informativeness, certificate leave-one-term-out, coverage–risk curves, control-plane audits, screening, and the complete cost ledger are reported in the supplementary material.

5 Limitations

Verdi's guarantees are conditional on a complete goal contract, a valid evaluator, and a correct evidence policy. Fingerprints are local and must be recomputed after major architectural changes. Early archives inherit the limits of observational priors and single-laboratory coverage, so distances, abstention rates, and collision statistics may shift with broader contributors. RoboCoin covers one dataset family and base model; it does not establish adaptation to arbitrary embodiments. H/I/E single-axis controls reduce confounding but do not by themselves establish causal identification.

6 Conclusion

We introduced Verdi, a verifiable differential-repair architecture. IRG ranks typed repair hypotheses across backbones; compilation, the six-term certificate, and target-side verification decide whether transfer is allowed. Settled positive, null, harmful, and interaction outcomes update WMOM, while failed transfers refine the diagnostic basis.

We demonstrated failure-specific repair, held-out certified transfer, and RoboCoin adaptation. Across these settings, Verdi reuses settled effects without hiding protected regressions or null results. Broader model families, uncertainty calibration, and contradiction-aware scheduling remain important directions for future work and future studies.

Ethics Statement

Verdi improves auditability but does not guarantee truth; results require independent replication, human review, and disclosure of generative-agent use. Training jobs, repository edits, and robot access require isolated credentials, least privilege, sandboxing, human approval, and an independent safety layer. Verify licenses and privacy for robot data/checkpoints, record provenance without secrets, assess dual-use risks, and use staged evaluation with explicit compute accounting.

Reproducibility Statement

Baseline and repair arms share initialization, steps, data, evaluator, paired contexts/seeds, and nominal allowance; measured costs are separate. Fixed gates, receipts, and code versions are logged; details are in Appendix B. Base models and datasets are publicly available.

References

AutoResearchClaw Team. Autoresearchclaw: Autonomous self-evolving multi-stage research pipeline. *arXiv preprint*, 2025.

Joeran Beel, Min-Yen Kan, and Moritz Baumgart. Evaluating sakana's ai scientist: Bold claims, mixed results, and a promising future? *ACM SIGIR Forum*, 2025. doi: 10.1145/3769733.376974.

Jun Shern Chan, Neil Chowdhury, Oliver Jaffe, James Aung, Dane Sherburn, Evan Mays, Giulio Starace, Kevin Liu, Leon Maksin, Tejal Patwardhan, Lilian Weng, and Aleksander Mądry. Mle-bench: Evaluating machine learning agents on machine learning engineering. In *International Conference on Learning Representations*, 2025.

GigaAI. Gigaworld-0: A large-scale world model and analysis of metric correlation structure. *arXiv preprint*, 2025.

Google DeepMind. Genie 3: A new frontier for world models. Technical report, 2025.

Yanjiang Guo, Lucy Xiaoyang Shi, Jianyu Chen, and Chelsea Finn. Ctrl-world: A controllable generative world model for robot manipulation. *arXiv preprint arXiv:2510.10125*, 2025.

David Ha and Jürgen Schmidhuber. World models. *arXiv preprint arXiv:1803.10122*, 2018.

Danijar Hafner, Timothy Lillicrap, Jimmy Ba, and Mohammad Norouzi. Dream to control: Learning behaviors by latent imagination. In *International Conference on Learning Representations*, 2020.

Danijar Hafner, Jurgis Pasukonis, Jimmy Ba, and Timothy Lillicrap. Mastering diverse control tasks through world models. *Nature*, 640(8059):647–653, 2025. doi: 10.1038/s41586-025-08744-2.

Yuci Han and Alper Yilmaz. Enhancing policy learning with world-action model. *arXiv preprint arXiv:2603.28955*, 2026.

Qian Huang, Jian Vora, Percy Liang, and Jure Leskovec. Mlagentbench: Evaluating language agents on machine learning experimentation. *arXiv preprint arXiv:2310.03302*, 2024.

Xun Huang, Zhengqi Li, Guande He, Mingyuan Zhou, and Eli Shechtman. Self forcing: Bridging the train-test gap in autoregressive video diffusion. In *Advances in Neural Information Processing Systems*, 2025.

Bo Jiang, Depu Meng, Yihan Hu, Yichen Xie, Tianshuo Xu, and Wei Zhan. Lamo: Self-supervised latent motion priors for physical realism in video generation. *arXiv preprint arXiv:2605.23878*, 2026.

Andrej Karpathy. autoresearch: Ai agents running research on single-gpu training automatically. `https://github.com/karpathy/autoresearch`, 2026.

Alexander Khazatsky, Karl Pertsch, Suraj Nair, Aditya Balakrishna, Sudeep Dasari, Siddharth Karamcheti, Soroush Nasiriany, Mohan Kumar Srirama, Lawrence Yunliang Chen, Kirsty Ellis, et al. Droid: A large-scale in-the-wild robot manipulation dataset. In *Robotics: Science and Systems*, 2024.

Ruiying Li, Yunlang Zhou, YuYao Zhu, Kylin Chen, Jingyuan Wang, Sukai Wang, Kongtao Hu, Minhui Yu, Bowen Jiang, Zhan Su, Jiayao Ma, Xin He, Yongjian Shen, Yang Yang, Guanghui Ren, Maoqing Yao, Wenhao Wang, and Yao Mu. Roboclaw: An agentic framework for scalable long-horizon robotic tasks. *arXiv preprint arXiv:2603.11558*, 2026.

Chris Lu, Cong Lu, Robert Tjarko Lange, Jakob Foerster, Jeff Clune, and David Ha. The ai scientist: Towards fully automated open-ended scientific discovery. *arXiv preprint arXiv:2408.06292*, 2024.

Alexander Novikov et al. Alphaevolve: A coding agent for scientific and algorithmic discovery. *arXiv preprint arXiv:2506.13139*, 2025.

NVIDIA, Niket Agarwal, Arslan Ali, Maciej Bala, Yogesh Balaji, et al. Cosmos world foundation model platform for physical ai. *arXiv preprint arXiv:2501.03575*, 2025.

Maxime Oquab, Timothée Darcet, Théo Moutakanni, Huy Vo, Marc Szafraniec, Vasil Khalidov, Pierre Fernandez, Daniel Haziza, Francisco Massa, Alaaeldin El-Nouby, et al. Dinov2: Learning robust visual features without supervision. *Transactions on Machine Learning Research*, 2024.

Samuel Schmidgall, Yusheng Su, Ze Wang, Ximeng Sun, Jialian Wu, Xiaodong Yu, Jiang Liu, Michael Moor, Zicheng Liu, and Emad Barsoum. Agent laboratory: Using llm agents as research assistants. *arXiv preprint arXiv:2501.04227*, 2025.

Yuqing Shang, Zonghao Li, Yuchen Ma, Weijie Su, Xiaobo Jin, Zan Wang, Li Jin, Xin Zhang, Yansong Tang, Hao Su, et al. Worldarena: A unified benchmark for evaluating perception and functional utility of embodied world models. *arXiv preprint arXiv:2602.08971*, 2026a.

Yuqing Shang et al. Worldarena 2.0: Extending embodied world model benchmarking on modality, functionality and platform. *arXiv preprint arXiv:2605.17912*, 2026b.

Zachary S. Siegel, Sayash Kapoor, Nitya Nadgir, Benedikt Stroebl, and Arvind Narayanan. Core-bench: Fostering the credibility of published research through a computational reproducibility agent benchmark. *arXiv preprint arXiv:2409.11363*, 2024.

Giulio Starace, Oliver Jaffe, Dane Sherburn, James Aung, Jun Shern Chan, Leon Maksin, Rachel Dias, Evan Mays, Benjamin Kinsella, Wyatt Thompson, Johannes Heidecke, Amelia Glaese, and Tejal Patwardhan. Paperbench: Evaluating ai's ability to replicate ai research. *arXiv preprint arXiv:2504.01848*, 2025.

Homer Walke, Kevin Black, Abraham Lee, Moo Jin Kim, Max Du, Chongyi Zheng, Tony Zhao, Philippe Hansen-Estruch, Quan Vuong, Andre He, Vivek Myers, Kuan Fang, Chelsea Finn, and Sergey Levine. Bridgedata v2: A dataset for robot learning at scale. *arXiv preprint arXiv:2308.12952*, 2023.

Shihan Wu, Xuecheng Liu, Shaoxuan Xie, Pengwei Wang, Xinghang Li, et al. Robocoin: An open-sourced bimanual robotic data collection for integrated manipulation. *arXiv preprint arXiv:2511.17441*, 2025.

Jia Xie, Tonghe Zhang, Haotian Lin, Letian Fu, Haoru Xue, Jalen Lu, Yi Yang, Cunxi Dai, Zi Wang, Jimmy Wu, Guanzhi Wang, S. Shankar Sastry, Ken Goldberg, Linxi Fan, Yuke Zhu, and Guanya Shi. Enpire: Agentic robot policy self-improvement in the real world. `https://research.nvidia.com/labs/gear/enpire/`, 2026.

John Yang, Carlos E. Jimenez, Alexander Wettig, Kilian Lieret, Shunyu Yao, Karthik Narasimhan, and Ofir Press. Swe-agent: Agent-computer interfaces enable automated software engineering. *arXiv preprint arXiv:2405.15793*, 2024.

Shijie Yue et al. Ewmbench: Evaluating scene, motion, and semantic quality in embodied world models. *arXiv preprint arXiv:2505.09694*, 2025.

Jenny Zhang, Shengran Hu, Cong Lu, Jeff Clune, and Robert Tjarko Lange. Darwin-gödel machine: Open-ended self-improving agents. *arXiv preprint arXiv:2505.22954*, 2025.

Fangyuan Zhu et al. Irasim: Learning interactive real-robot action simulators. *arXiv preprint*, 2025a.

Minjun Zhu, Qiujie Xie, Yixuan Weng, Jian Wu, Zhen Lin, Linyi Yang, and Yue Zhang. Ai scientists fail without strong implementation capability. *arXiv preprint arXiv:2506.01372*, 2025b.

A Formal Method Details

We study automated improvement of a pretrained world model under a user-specified goal and a finite nominal verification allowance. Our key view is that repairability can be measured through a local intervention geometry. Semantically dosed, inference-only intervention paths yield paired response Jacobians; their induced metric describes which repair directions produce distinguishable behavioral changes. VERDI organizes these uncertainty-bearing charts into an Interventional Repair Geometry (IRG), transports local repair-effect fields only through contract-checked, empirically bounded-distortion chart maps, and abstains outside calibrated support. When geometric neighbors exhibit statistically opposing repair effects, the failed transfer becomes a counterexample that drives regret-gated atlas refinement without changing the campaign verifier.

A.1 Goal-Conditioned World-Model Improvement

A campaign is a tuple $\mathcal{C} = (b, \theta_0, \mathcal{D}, G, V_G, \mathcal{B})$, where b is a backbone with pretrained parameters θ_0, $\mathcal{D}$ is the campaign data, G is a goal specification, V_G is an independent verifier, and $\mathcal{B}$ is a nominal resource allowance. The goal specifies a primary utility U_G, evaluation contexts $x \sim \mathcal{D}^{\mathrm{ver}}$, horizons $h \in \mathcal{H}_G$, and a set of validity constraints v_j. For a candidate model θ, we define

$$J_G(\theta) = \sum_{h \in \mathcal{H}_G} w_h \, \mathbb{E}_{x \sim \mathcal{D}^{\mathrm{ver}}}[U_G(\theta; x, h)], \quad \text{s.t.} \quad v_j(\theta) \le 0 \ \ \forall j. \tag{10}$$

The constraints prevent a nominal metric gain from being obtained by invalid behavior, such as ignoring actions or collapsing motion. In our instantiation, the outcome schema and its gates follow a multi-dimensional world-model evaluation suite (WorldArena in our experiments), and the gate thresholds encode empirically verified metric correlation structures: metrics reported to co-vary positively or negatively with the primary metric must stay within tolerance. Thus improving the primary metric cannot silently sacrifice its known trade-off partners. All comparisons use paired evaluation contexts and seeds. For intervention set S, we retain $\boldsymbol{y}(S) = [\Delta J_G(S), \{\Delta U_k(S,h)\}_{k,h}, \{v_j(S)\}_j, C(S)]$, where $C(S)$ is measured cost. This vector, rather than a single scalar score, is retained because an intervention may improve short-horizon fidelity while damaging long-horizon dynamics or behavioral validity.

A.2 Interventional Repair Geometry

A static probe bank first extracts $\boldsymbol{z}_x = P_v(\theta, \mathcal{D}^{\mathrm{dev}}, G)$ for campaign instance x. These cheap observations remain useful covariates for effect prediction, but are not treated as geometric coordinates because their scales need not be invariant across backbones.

The backbone adapter declares a capability vector $\boldsymbol{c}_x$ and a set of typed intervention paths $\mathcal{I}_{b,s}(d)$ with semantic dose d and $\mathcal{I}_{b,s}(0) = \mathrm{Id}$. A path must be inference-only, reversible, paired with the same seeds and trajectories as the baseline, and measurable at at least two nonzero doses. Examples include action scaling, controlled context retention, first-frame anchoring strength, and sampler-noise stress. Training losses and data reweighting are excluded because their optimization response is neither cheap nor dose-comparable across backbones.

Let $\boldsymbol{q}_x(\boldsymbol{d})$ denote the robustly standardized vector of goal, diagnostic, and validity outcomes under intervention dose vector $\boldsymbol{d}$. In chart q, paired central differences estimate the local response Jacobian

$$\boldsymbol{J}_x^q[:, s] = \left. \frac{\partial \mathbb{E}[\boldsymbol{q}_x(\boldsymbol{d})]}{\partial d_s} \right|_{\boldsymbol{d}=0} \approx \frac{\widehat{\boldsymbol{q}}_x(+\delta_s) - \widehat{\boldsymbol{q}}_x(-\delta_s)}{2\delta_s}. \tag{11}$$

For a one-sided path, the compiler records a normalized secant instead. A small dose grid checks that the response is locally stable; paths whose finite-difference slope changes beyond tolerance remain finite-dose probes rather than local directions.

The Jacobian induces a weighted repair metric on the intervention frame,

$$\boldsymbol{G}_x^q = (\boldsymbol{J}_x^q)^\top \boldsymbol{W}_q \boldsymbol{J}_x^q + \lambda \boldsymbol{I}, \qquad \boldsymbol{r}_x^q = \mathrm{vec}(\boldsymbol{W}_q^{1/2} \boldsymbol{J}_x^q), \tag{12}$$

where $\boldsymbol{W}_q$ is fixed by the goal and outcome schema, not fitted to the test campaign. Bootstrap repeats provide uncertainty $\boldsymbol{\Sigma}_x^q$. A chart is simply the tuple of goal schema, outcome schema, capability class, and supported intervention frame; compatible charts form the IRG. Static probes $\boldsymbol{z}_x$, capabilities $\boldsymbol{c}_x$, and missingness metadata condition the effect predictor but are not mixed into

the repair coordinates. Starting from a small canonical frame, additional directions are retained only when nested cross-domain replay shows that their reduction in repair-selection regret repays their probing cost. Thus IRG is optimized for future repair decisions, not for reconstructing an unobserved physical mechanism.

A.3 Typed Interventions and Semantics-Preserving Compilation

An intervention is not a free-form code patch. It is a typed descriptor $a = (\ell_a, \psi_a, \omega_a, d_a, s_a, \mathsf{pre}_a, \mathsf{inv}_a, \boldsymbol{\chi}_a)$, where ℓ_a is a required hook type, ψ_a is the transformation, ω_a is its scope, d_a is a behaviorally defined dose, s_a is a schedule, pre_a lists applicability conditions, inv_a lists semantic invariants, and $\boldsymbol{\chi}_a$ is a falsifiable prediction over repair-response and horizon behavior. Examples of invariants include preserving the data split, applying a loss to the declared tensor, or restricting a sampler change to inference. In our system, verified repair methods are stored as such atomic descriptors—for example, feature-conditioning via pretrained visual encoders—each annotated with the task types and capability classes where it was confirmed, null, or harmful.

Each backbone exposes a capability vector $\boldsymbol{c}_b$ and a typed hook inventory. A compiler maps a to $\Gamma_b(a) = (\delta_a, r_a)$ only if $\mathsf{Sat}(r_a, \mathsf{pre}_a, \mathsf{inv}_a, \boldsymbol{c}_b) = 1$, where δ_a is the executable patch and r_a is a receipt containing hook-contract tests, dose units and direction, outcome semantics, and invariant checks. Compilation fails rather than silently approximating an unavailable mechanism. For cross-backbone comparison, compatible receipts propose a partial intervention-axis map $\boldsymbol{T}_{i\to x}$ and outcome map $\boldsymbol{B}_{i\to x}$; these maps are hypotheses that must pass empirical chart-alignment tests, not proofs supplied by code similarity.

A.4 Capability-Preserving Geometric Transfer

Compatible receipts define a shared chart and maps $\boldsymbol{T}_{i\to x}$ and $\boldsymbol{B}_{i\to x}$. We reject a map when paired anchor contexts do not preserve the measured response directions:

$$e_{\mathrm{align}}(i,x) = \frac{\|\boldsymbol{J}_x\boldsymbol{T}_{i\to x} - \boldsymbol{B}_{i\to x}\boldsymbol{J}_i\|_F}{\|\boldsymbol{J}_x\boldsymbol{T}_{i\to x}\|_F + \|\boldsymbol{B}_{i\to x}\boldsymbol{J}_i\|_F + \epsilon}. \tag{13}$$

Within a fixed shared chart, a simple fixed, uncertainty-normalized distance defines repair neighbors:

$$d^2_{\mathrm{IRG}}(x,i) = (\boldsymbol{r}_x - \widetilde{\boldsymbol{r}}_i)^\top \boldsymbol{W}_q^{\mathrm{dist}}(\boldsymbol{r}_x - \widetilde{\boldsymbol{r}}_i) + \lambda_c d^2_{\mathrm{cap}}(\boldsymbol{c}_x, \boldsymbol{c}_i), \tag{14}$$

where tildes denote transported coordinates and $\boldsymbol{W}_q^{\mathrm{dist}}$ is fixed from the frozen, target-independent archive M_k^{full} before target evaluation, with noisy coordinates downweighted. The archive contains shared prior entries and all eligible pre-target source campaigns; target-specific records and post-evaluation updates are excluded. Each repair a defines a local effect function τ_a over this space, estimated only from campaigns satisfying the same typed repair contract. Thus transfer predicts a context-local effect, not the universal validity of a recipe.

A weighted local predictor gives mean effect $\widehat{\mu}_a(x)$ and uncertainty $\widehat{\sigma}_a(x)$. The geometry version, predictor, and repair set are frozen before an independent group-calibration split constructs a one-sided lower bound $L_a(x)$. Campaigns, not frames, are calibration units, and a changed IRG version invalidates the old bound.

Transfer is licensed only by a certificate. We write every protected constraint as a violation v_j: $v_j \le 0$ passes and $v_j > 0$ fails. Formally,

$$\begin{aligned}\mathsf{Cert}_{\mathrm{app}}(x,a) = \mathbb{I}[\mathsf{compile} = 1]\mathbb{I}[\mathsf{overlap} \ge \rho_{\min}]\mathbb{I}[N_{\mathrm{eff}} \ge n_{\min}] \\ \cdot \mathbb{I}[e_{\mathrm{align}} \le \epsilon_{\mathrm{align}}]\mathbb{I}[\mathsf{sign_agree} \ge \gamma]\mathbb{I}[L_a(x) > \delta_G] \\ \cdot \prod_j \mathbb{I}[\widehat{v}_{t,j}(a) \le 0],\end{aligned} \tag{15}$$

The six terms correspond one-to-one to the six failure modes: compilation failure, insufficient support overlap, insufficient evidence, response misalignment, sign disagreement, and insufficient gain over cold start. If any term fails, the system abstains from effect transfer. It may still reuse lower levels of infrastructure: L0 transfers only the loop, L1 transfers compatible diagnostics, L2 transfers a compiled intervention, and L3 additionally transfers an effect prior under Eq. 15. Imported evidence changes candidate order but never bypasses target-domain verification.

Among valid candidates, the online selector is deliberately simple:

$$a_t = \arg\max_{a \in \mathcal{A}_t} \frac{\widehat{\mu}_a(x) + \beta_t \widehat{\sigma}_a(x)}{\widehat{C}(a)}. \tag{16}$$

Validity and capability constraints define $\mathcal{A}_t$ and are not traded against reward through tunable penalties. A certified transfer initializes the posterior; an abstention uses a cold prior.

We use progressive fidelity: a low-cost paired screen only estimates effect direction, while promoted candidates receive paired multi-seed confirmation on held-out contexts. Screening evidence may update search uncertainty but cannot create a confirmed effect record.

A.5 Factorized Intervention Effects

Composite interventions are useful for exploration but ambiguous for attribution. If a set S is promising, VERDI schedules matched contrasts using common seeds and examples. For primitive $i \in S$, its local interventional credit is estimated from the available factorial contrasts

$$\widehat{\tau}_i = \sum_{A \in \mathcal{F}_i} w_A \left[\overline{Y}(A \cup \{i\}) - \overline{Y}(A) \right], \tag{17}$$

where $\mathcal{F}_i \subseteq 2^{S \setminus \{i\}}$ contains matched contexts. With all subsets, Eq. 17 recovers Shapley-style factorial credit; under a smaller allowance, leave-one-out effects are retained explicitly as conditional rather than universal effects. Pairwise interaction is stored separately as $\widehat{\tau}_{ij}^{\text{int}} = \overline{Y}(\{i,j\}) - \overline{Y}(\{i\}) - \overline{Y}(\{j\}) + \overline{Y}(\varnothing)$.

An entry becomes a *confirmed local intervention effect* only when its lower confidence bound exceeds the campaign threshold, every validity gate passes, protected metrics remain within tolerance, and the result replicates over the required seeds. Its context records the IRG chart, backbone capabilities, data regime, goal, and horizon range. The Intervention-Effect Memory (IEM) layer of the World Model Optimization Memory (WMOM) stores confirmed, null, rejected, and interaction effects. We claim only randomized paired local effects under this context, not discovery of a complete causal graph.

A.6 Counterexample-Driven IRG Evolution

A fixed atlas can alias distinct repair states. We expose this failure as a *repair collision*: two campaigns with the same goal schema and shared repair support are close in the current IRG, yet a non-negligible repair has a high-confidence opposing effect. Let

$$\begin{aligned} \mathcal{K}_\tau = \Big\{ (i,j) : d_{\text{IRG}}(i,j) \le \tau_q, \\ \exists a \in \mathcal{A}_i \cap \mathcal{A}_j : \\ \Pr(\tau_{i,a}\tau_{j,a} < 0 \mid \mathcal{E}) \ge 1 - \alpha_c, \\ \min(|\tau_{i,a}|, |\tau_{j,a}|) > \epsilon_c \Big\}. \end{aligned} \tag{18}$$

Such a collision is evidence of repair-relevant aliasing, not proof that a hidden mechanism has been identified. In our experience this arises, for instance, when a feature-conditioning repair improves soft-body scenes but degrades several metrics on rigid-body scenes whose static descriptions look similar. Rather than expanding the library on a schedule, the system requests a new diagnostic direction only when collisions survive uncertainty and schema checks. From staged probes or sentinels, it selects

$$s^\star = \arg\max_s \frac{\text{LCB}\Big[\widehat{\mathcal{R}}_{\text{nested}}(\mathcal{S}) - \widehat{\mathcal{R}}_{\text{nested}}(\mathcal{S} \cup \{s\}) \mid \mathcal{K}_\tau\Big]}{C_{\text{probe}}(s)}, \tag{19}$$

which directly targets future repair-selection errors rather than raw feature separation. Because collisions are screened over many campaign pairs, we control the false discovery rate over $\mathcal{K}_\tau$ and shrink small-sample effect estimates toward the chart mean before any direction is staged. The inner replay learns the frame and effect predictor; disjoint promotion domains estimate regret and calibration. Repeated search failure with no representational collision instead signals a missing repair skill and opens the primitive-staging path.

Generated candidates do not immediately control live search. They first run in shadow mode under nested leave-one-domain/backbone-out replay and enter the next version only if they lower selection regret and trials-to-first-positive without worsening calibration or the frozen regression battery. Verdict-facing probes and V_G remain frozen within a campaign. Thus capability acquisition is open, but authority is granted only through out-of-domain predictive value.

Algorithm 1 Repair-Geometry Learning and Selective Transfer in VERDI

Require: Campaign $\mathcal{C}$, probes P_v, intervention frame $\mathcal{S}_v$, repair registry $\mathcal{R}_v$, IEM layer $\mathcal{E}$
Ensure: Verified recipe $A^\star$, updated $\mathcal{E}$, staged capabilities

Instantiate and freeze verifier V_G; audit backbone capabilities $\boldsymbol{c}_b$
Measure static covariates $\boldsymbol{z}$ and compile the supported intervention frame $\mathcal{S}_b \subseteq \mathcal{S}_v$
Run paired dose paths; estimate $(\boldsymbol{J}_x, \boldsymbol{G}_x, \boldsymbol{\Sigma}_x)$ and locality residuals
for each typed repair $a \in \mathcal{R}_v$ **do**
    Compile a and chart maps; reject failed contracts or excessive map distortion
    Evaluate $\mathsf{Cert}(x, a)$; initialize a transported-field or cold posterior
end for
Let $\mathcal{A}$ be the remaining compiled candidates
while remaining nominal allowance is sufficient for a valid trial **do**
    Select a from $\mathcal{A}$ using Eq. 16
    Run the cheapest admissible paired trial; settle response $\boldsymbol{y}(a)$ and receipts
    Update the local posterior and the IEM layer of WMOM $\mathcal{E}$
    if a passes the low-cost promotion rule **then**
        Run held-out multi-seed confirmation under frozen V_G
        if a is composite and remains positive **then**
            Schedule matched factorial or leave-one-out contrasts
        end if
        Mark only replicated, gate-valid positive effects as confirmed
    end if
    if new repair collisions $\mathcal{K}_\tau$ appear **then**
        Stage the direction maximizing nested-replay regret reduction in Eq. 19
    else if search stagnates without a collision **then**
        Stage a new repair primitive rather than rewriting the geometry
    end if
end while
Shadow-replay staged capabilities on disjoint promotion domains; queue only regret- and calibration-valid passes for version $v + 1$
return best verified recipe $A^\star$, $\mathcal{E}$, and the staged queue

What is learned. The final product is not only a tuned checkpoint. It is a calibrated repair geometry, verified recipes, local intervention effects and interactions, abstention certificates, negative results, and replay-tested capability candidates. Every settled experiment changes the local effect model, reveals a transfer boundary, or exposes a collision that can drive the next IRG revision.

B ABLATION AND AUDIT DETAILS

Each subsection below isolates one design decision and states up front the claim it supports. Unless noted otherwise, all numbers are means over three seeds, computed on paired evaluation contexts with the frozen campaign verifier V_G; in each table, the best value per column is typeset in bold. We commit to reporting whichever outcome obtains; where an ablation does not favor a design choice (e.g., the selector in §B.6), we say so rather than re-framing the result.

Archive ablation convention. For held-out target t in fold k, the complete archive is denoted M_k^{full} and is frozen before target-side evaluation. It contains the shared prior archive and all eligible pre-target source campaigns; target-specific records, target-side calibration, tuning decisions, and post-evaluation updates are excluded. The archive ablation compares M_k^{full} against $M_k^{\text{empty}} = \varnothing$ (the cold-start arm). All other ablations keep M_k^{full} fixed and vary only the named component; source and target protocols, budgets, and verifiers remain unchanged.

Eight-environment testbed (ACWM-Phys). The fingerprint and distance analyses of this appendix use an eight-environment testbed built on ACWM-Phys, a compact action-conditioned world model, spanning rigid-body contact (push/stack cube), deformable and granular media (cloth, rope, sand), fluid transport (pour water), and articulated dynamics (robot arm, reacher). We use ACWM-Phys as a compact seed slice for the initial development of the audit machinery: its small scale makes paired multi-seed confirmation, the exhaustive reference evaluation of §B.6, and the planted-fault audits of §B.5 feasible at full fidelity. This seed slice is not the complete prior knowledge base. The shared

Table 5: **Shared prior knowledge bases available before held-out transfer.** ACWM-Phys is the compact seed slice used for early protocol and audit development; additional completed backbone campaigns are part of the shared prior archive and their exact fold-specific inclusion is recorded in the campaign ledger.

Archive component	Role	Inventory / status
ACWM-Phys seed campaigns	Compact initial memory for fingerprint, gate, certificate, and audit development	Eight environments; pre-LOBO seed slice
Other shared backbone archives	Settled prior entries from completed or registered campaigns; examples: Ctrl-World, Cosmos-Predict 2, Cosmos3, IRASim (Zhu et al., 2025a), OccWorld, DreamerV3, TD-MPC2, and DINO-WM/V-JEPA 2	*Included in M_k^{full}; exact snapshot and fold IDs are recorded in the ledger*

prior archive also contains settled campaigns from other backbones; together with all eligible source campaigns, these entries constitute M_k^{full}. Its high-level inventory is summarized in Table 5, with the campaign-level ledger retained separately. For held-out transfer, the archive snapshot and selector calibration are frozen before target-side evaluation, and target results are added only after the fold is settled. Cross-backbone behavior of the geometry is evaluated separately in the main campaigns (§4).

B.1 Fingerprint Informativeness

Claim supported (§3.3). The IRG fingerprint must carry more repair-relevant information than cheaper similarity signals. We ask each candidate representation to predict, for held-out campaign pairs, whether a confirmed repair will have a positive effect on a target backbone (sign agreement). Competitors: environment labels only; static probe covariates $\boldsymbol{z}_x$; raw (unweighted) response vectors with a flat Euclidean distance; and the full fingerprint with the induced metric of Eq. 12 and dose calibration.

Table 6: Repair-effect sign agreement on held-out campaign pairs, by representation. The full fingerprint row corresponds to the informativeness results reported in the main text.

Representation	Sign agreement ↑
IRG fingerprint (full)	**0.83**
Raw response + flat distance	0.71
Static probes $\boldsymbol{z}_x$ only	0.65
Environment labels only	0.58

Table 6 shows a clear ordering. The gap between the full fingerprint and the raw-response/flat-distance variant isolates the contribution of the weighted induced metric and dose calibration; the gap to static probes and environment labels shows that interventional response structure, not surface covariates, carries the repair-relevant signal. Sign agreement alone, however, does not establish that the fingerprint is implicated in selecting repairs; the end-to-end selection-source ablation is reported in Table 14.

B.2 Agent-Level Controls Under Matched Budget

Claim supported (§4.5). The ablations above remove individual components of VERDI ; here we ask the complementary question: does the *architecture as a whole* outperform an agent with the same nominal allowance that lacks it? All arms share the same LLM (frozen version), the same typed repair registry, the same evaluation protocol with paired contexts and seeds, and the same nominal per-campaign search allowance ($\mathcal{B} = 200$ GPU-h; overruns are reported rather than censored). Arms differ only in which machinery mediates proposal, licensing, and settlement. The bare agent proposes and executes repairs from the registry freely, without fingerprints, certificates, or abstention; the generic research-agent loop follows the standard propose–implement–run–observe cycle used by ML-benchmark agent scaffolds. We additionally include two trivial selectors to exclude the explanations



Figure 5: **Dose-response slopes across eight environments and seven probe directions (ACWM-Phys testbed).** All axes and the color scale are described here rather than in the panel. Each cell is the paired finite-difference slope of the primary utility U_G per unit dose—same seeds and trajectories, with and without a small dose—robustly standardized (§A.2); rows (top to bottom) are the eight environments (push cube, stack cube, push rope, cloth move, push sand, pour water, robot arm, reacher), columns (left to right) the probe directions (action amplify, action attenuate, self-rollout mix, motion scale, action-time mix, event align, action align). Blue marks a positive slope, orange a negative one; saturation encodes magnitude ($|z| \approx 2$: strong response; $|z| \approx 0$: the path does not move U_G). Paths outside the supported intervention frame are marked $\times$. Columns 1–2 are the two one-sided directions of the canonical action-scaling path, recorded as normalized secants (§A.2); columns 3–4 complete the canonical frame; columns 5–7 are diagnostic directions admitted in IRG v2 through collision-driven staging, whose ablation is reported in main-text Table 3.

that lucky guessing or a single universally effective repair drives our results: a frequency prior that always deploys the historically most-confirmed repair, and uniform random selection. End-to-end metrics follow main-text Table 4.

Table 7: Agent-level controls under matched nominal allowance (200 GPU-h per campaign; same LLM and repair registry). Means over three backbones and three seeds.

Agent configuration	Trials-to-first-pos. ↓	Search cost (GPU-h) ↓	Neg. transfer ↓	Prot. viol. ↓
VERDI (full)	**3.6**	**96**	**0.06**	**0.03**
w/o certificates (IRG only)	4.3	128	0.21	0.14
w/o IRG (cert. over text-sim. neighbors)	4.8	142	0.18	0.11
Bare LLM agent (same pool, free proposal)	5.9	187	0.31	0.26
Generic research-agent loop	6.4	213	0.36	0.29
Frequency prior (most-confirmed repair)	5.2	164	0.29	0.22
Random selection	8.7	246	0.38	0.33

Table 7 shows that unconstrained agents are not dramatically slower to a first positive—the bare agent reaches one in 5.9 trials, echoing the unconditional-transfer row of main-text Table 4—but they pay for it elsewhere: negative-transfer and protected-violation rates are 5–8$\times$ higher than the full system, and total search cost roughly doubles because harmful attempts consume budget that certificates would have reserved. Removing either the certificates or the IRG degrades exactly the metric the removed component was designed to protect, consistent with Table 8 and main-text Table 3.

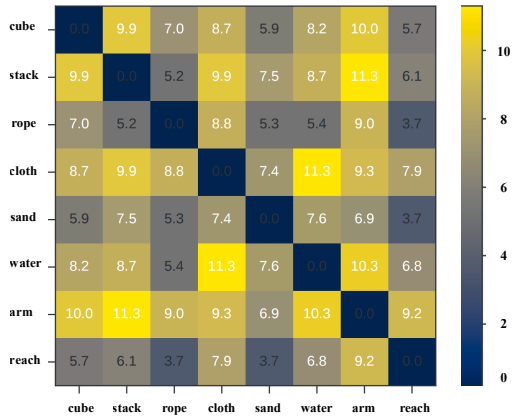


Figure 6: **Pairwise IRG distances between environments (ACWM-Phys testbed).** All axes and the color scale are described here rather than in the panel. Each cell is the IRG distance d_{IRG} (Eq. 14) between two environments (same row/column order as Fig. 5); the diagonal is zero by construction, and cell brightness encodes distance (dark ≈ 0 to bright ≈ 11; the collision-screening neighbor threshold τ_q of Eq. 18 is 7.5). Distances are computed from the full repair fingerprint $\boldsymbol{r}_x = \mathrm{vec}(\boldsymbol{W}_q^{1/2}\boldsymbol{J}_x)$ over all goal, diagnostic, and validity outcomes (Eq. 12); Fig. 5 displays one outcome row of the underlying Jacobian. The structure recovers physically meaningful groupings—granular and topology-driven tasks (sand, rope, $d = 5.3$) lie well inside the neighbor range, whereas superficially similar rigid-body tasks (cube, stack, $d = 9.9$) are clearly separated—and defines the repair neighbors over which local effect fields are estimated (§A.4).

The frequency-prior arm performs respectably on speed, confirming that the registry contains strong repairs, but it cannot avoid the repair–backbone mismatches that certificates filter out.

As an external reference, two engineers experienced with video world models were given the same registry, nominal allowance, and verifier on Ctrl-World. They reached first-positive in 3.9 trials with protected violation 0.05—comparable to VERDI —but required approximately 14 hours of expert wall-clock per campaign and did not produce transferable records: repeating the exercise on Cosmos-Predict 2 reset their search nearly from scratch (10.8 trials), whereas the system's certified transfer carried over at 3.6 trials. We do not claim superhuman repair ability; the comparison indicates that the system's advantage lies in accumulating transferable evidence rather than in exceeding expert intuition on any single campaign.

B.3 CERTIFICATE LEAVE-ONE-TERM-OUT

Claim supported (§3.5, §4.5). Each of the six certificate terms in Eq. 7 must guard a distinct failure mode. We disable one term at a time and measure the corresponding failure rate over the LOBO replay of main-text Table 4. Failure modes: *compilation failure* (the candidate cannot be compiled under the target contract), *insufficient support overlap* (the target lies outside calibrated support), *insufficient evidence* (the target lacks the diagnosed deficiency), *response misalignment* (target responses do not align with the source effect), *sign disagreement* (neighbors disagree on direction), and *insufficient gain over cold start* (the imported prior does not beat the cold posterior).

Table 8 shows that no term is redundant: disabling any single one raises its guarded failure mode to 2.5–4.7$\times$ the full-certificate rate, with response alignment (e_{align}) and the calibrated effect bound (L_a) carrying the largest loads. Note that the diagnosis check (compile/overlap) primarily prevents wasted budget rather than harmful records, which is why the abstention path in §A.4 falls back to a cold prior instead of blocking the campaign.

B.4 VALIDITY-GATE ABLATION AND THRESHOLD SENSITIVITY

Claim supported (§3.1, §4.1). The validity gates exist to prevent nominal primary-metric gains obtained by sacrificing correlated partner metrics. We compare the full gate set against removing the negatively correlated guard rails, and we re-calibrate every tolerance τ at $0.5\times$ and $2.0\times$ its default ($1.5\times$ the baseline seed-level standard deviation) to check that conclusions do not flip.

Table 8: Certificate leave-one-term-out. Each row disables exactly one term of Eq. 7; the reported rate is the failure mode that term is designed to guard. The full certificate row is the overall negative-transfer rate from main-text Table 4.

Disabled term	Exposed failure mode	Failure rate ↑
Full certificate (none disabled)	overall negative transfer	**0.06**
$\mathbb{I}[\mathsf{compile} = 1]$	compilation failure	0.19
$\mathbb{I}[\mathsf{overlap} \geq \rho_{\min}]$	insufficient support overlap	0.17
$\mathbb{I}[N_{\text{eff}} \geq n_{\min}]$	insufficient evidence	0.15
$\mathbb{I}[e_{\text{align}} \leq \epsilon_{\text{align}}]$	response misalignment	0.28
$\mathbb{I}[\mathsf{sign_agree} \geq \gamma]$	sign disagreement	0.18
$\mathbb{I}[L_a(x) > \delta_G]$	insufficient gain over cold start	0.24

Table 9: Validity-gate ablation and threshold sensitivity. Primary Δ is the mean primary-metric gain over gated campaign contexts; protected violation is the fraction of contexts where any protected metric exceeds tolerance; decision changed reports whether any campaign-level verdict (confirmed/null/rejected) flips relative to the default.

Configuration	Primary Δ ↑	Protected viol. ↓	Decision changed
Full gates ($\tau = 1.5\times$, default)	+12.78	**0.03**	–
No negative-correlation gates	+14.92	0.41	–
All tolerances at $0.5\times$	+11.86	0.04	no
All tolerances at $2.0\times$	+13.05	**0.03**	no

Table 9 shows the gates doing real work: removing them *raises* the headline primary gain (from $+12.78$ to $+14.92$) while protected-constraint violations rise $13\times$—precisely the silent trade-off the gates exist to expose. We deliberately keep the gated, smaller gain. Re-calibrating all tolerances by a factor of two in either direction changes no campaign verdict, indicating that our conclusions are not an artifact of the tolerance choice.

B.5 Control-Plane Ablation Under Planted Faults

Claim supported (§3.2, §4.1). The geometric-layer ablations measure repair quality; they do not measure whether the control layer—dual planes, receipts, H/I/E separation, progressive fidelity—actually prevents wrong conclusions. We therefore audit it under planted faults. We construct 30 trap episodes (six per type) spanning five failure modes drawn from our own failure taxonomy: (i) *evaluator leakage*, where the verification signal is contaminated by training context; (ii) *within-noise gain*, where the effect size is below seed-level standard deviation; (iii) *protected-metric sacrifice*, where the primary metric improves while a correlated partner degrades beyond tolerance; (iv) *confounded attribution*, where the apparent gain is produced by an uncontrolled factor (extended schedule); and (v) *single-seed fluke*, where one seed shows a large effect that does not replicate. Ten additional episodes contain genuine, gate-valid improvements. Episodes are interleaved and presented to each arm without labels; each arm must settle each episode into its memory as confirmed, null, or rejected. We report the false-conclusion rate (traps settled as confirmed) and the missed-genuine rate, averaged over three seeds on Ctrl-World and Cosmos-Predict 2.

Table 10: Control-plane ablation on 30 planted-fault and 10 genuine-improvement episodes. False conclusion = trap settled as *confirmed*; missed genuine = valid improvement settled as *null/rejected*. Overhead is the mean extra compute per episode relative to direct settlement.

Control configuration	False conclusion ↓	Missed genuine ↓	Overhead (GPU-h/ep.)
Full control plane	**0.07**	0.10	+6.2
w/o H/I/E separation	0.28	0.09	+4.8
w/o validity gates	0.41	0.08	+5.1
w/o progressive fidelity	0.33	0.07	−3.4
No control plane (direct settle)	0.52	**0.04**	0.0

Table 10 shows the expected trade. Direct settlement misses almost nothing—it accepts nearly every episode—but settles over half of the planted faults as confirmed effects, and each such record would

have entered the Intervention-Effect Memory (IEM) layer of the World Model Optimization Memory (WMOM) as transferable evidence. The full control plane reduces false conclusions by $7.4\times$ at a cost of 6.2 GPU-h per episode and a modest increase in missed genuine effects (within-noise gains that require more seeds to promote). Removing H/I/E separation roughly quadruples false conclusions: when the same loop proposes, implements, and settles, confounded-attribution traps (type iv) are the most likely to pass. Removing progressive fidelity saves overhead but allows low-cost screens to create confirmed records directly, re-opening the fluke channel (type v).

B.6 Progressive-Fidelity Screening and Selector Ablation

Claim supported (§3.5, §3.6). The low-cost screen must retain genuinely effective repairs while saving evaluation budget, and the online selector of Eq. 16 must not be the source of the gains. We measure screen recall against exhaustive evaluation of all compiled candidates (the reference answer), then swap the selector for simpler alternatives while holding the screen fixed.

Table 11: Screening recall and selector ablation. Recall is the fraction of repairs confirmed by exhaustive evaluation that the screen retains for confirmation; cost is the mean measured C_{search} per campaign. The exhaustive row is the recall reference, not a deployable policy.

Strategy	Screen recall ↑	C_{search} (GPU-h) ↓
Exhaustive evaluation (reference)	1.00	480
Screen + UCB selector (default)	**0.94**	**205**
Screen + kNN selector	**0.94**	214
Screen + random selector	0.91	268

Table 11 shows that the screen retains 94% of exhaustively confirmed repairs at 43% of the evaluation cost. We report plainly that the selector is *not* the source of the gains: a kNN selector is within noise of UCB, and even random selection over screened candidates outperforms no screening. The savings come from the progressive-fidelity discipline itself—cheap paired screens plus held-out multi-seed confirmation—not from acquisition sophistication.

B.7 Cost Ledger

Claim supported (§4.5). Fingerprinting and screening incur upfront cost; this ledger accounts for it per campaign. Avoided spend is estimated from the cold-start trajectory of the same campaign (main-text Table 4) net of measured C_{overhead}. This ledger is separate from the main-text measured $C_{\mathrm{first+}}$.

Table 12: Per-campaign measured cost ledger (GPU-h). C_{overhead} = fingerprinting + screening + confirmation; it is reported separately from main-text $C_{\mathrm{first+}}$. Net saved = avoided spend − overhead.

Campaign	Fingerprinting	Screening	Confirmation	Overhead	Net saved
Ctrl-World	9	51	36	96	+96
Cosmos-Predict 2	11	74	88	173	+139
Cosmos-Predict 2.5	8	60	62	130	+132

Table 12 shows that fingerprinting costs only 8–11 GPU-h per campaign and is repaid within the first certified transfer; all three campaigns end net-positive. The ledger also makes the honest accounting visible: confirmation, not measurement, dominates overhead.

B.8 Budget Alignment

Fairness statement (§4). Every baseline and improved variant within a campaign uses identical training steps and data, with matched nominal hyperparameter-search allowance. Measured training compute and search overhead are reported separately, so differences in outcomes cannot be attributed to different schedules or search allowances.

B.9 Selector Source Ablation

The main-text selector summary is expanded here so that all retrieval baselines are auditable without consuming the nine-page main-text budget.

Table 13: Training-schedule alignment and measured compute for all backbone–repair comparisons.

Campaign	Train steps	Data	Compute (GPU-h, base vs. improved)	HP trials
Ctrl-World	200k	identical	420 vs. 425	12
Cosmos-Predict 2	50k	identical	380 vs. 386	10
Cosmos-Predict 2.5	50k	identical	390 vs. 394	10

Table 14: **Source of repair selection.** Only the selection signal changes across rows; the executor, repair registry, nominal allowance, and verifier are held fixed.

Selection source	Sign agreement ↑	Trials to positive ↓	Neg. transfer ↓	Protected violation ↓
Full intervention fingerprint	**0.83**	**3.6**	**0.06**	**0.03**
Learned model embedding	0.74	4.6	0.17	0.10
Raw response + flat distance	0.71	4.4	0.15	0.09
Static metadata nearest neighbor	0.65	5.1	0.21	0.13
Repair-text embedding	0.62	5.8	0.24	0.16
Frequency prior	0.57	5.2	0.29	0.22
Random selection	0.50	8.7	0.38	0.33

C Additional Backbone-Specific Experiments

The main text evaluates failure-specific repair, probe evolution, repair selection, and held-out transfer. This appendix retains the detailed backbone-specific experiments from the original manuscript: Ctrl-World, Cosmos-Predict 2, Cosmos3, downstream action generation, and RoboCoin adaptation. These studies provide concrete implementation and qualitative evidence, while the matched selection and transfer comparisons remain in the main text.

C.1 Extended Protocol

We treat VerdiWM as a research agent for a world model and evaluate its ability to propose minimal interventions targeted to the diagnosed failure of each backbone. To isolate the intervention itself, we preserve the original observation interface, tokenizer or VAE, decoder or renderer, data partition, and evaluation implementation unless a selected repair explicitly targets that component. The baseline is the original backbone without VerdiWM intervention, compared under the same data, matched training schedule, nominal search allowance, and evaluation protocol.

The instantiated repairs differ by diagnosed mechanism. Ctrl-World (Guo et al., 2025) receives a LaMo (Jiang et al., 2026)-style latent-motion prior for insufficient physical consistency; Cosmos-Predict 2 (NVIDIA et al., 2025) receives DINOv2 (Oquab et al., 2024) representation guidance (REP) for structural drift; Cosmos3 receives self-forcing (Huang et al., 2025) for train–inference mismatch during long-horizon rollout; and RoboCoin (Wu et al., 2025) uses an automatically constructed data and action-conditioning adapter. We report standard video metrics (PSNR, SSIM, LPIPS, and FID), WorldArena-style semantic, depth, flow, smoothness, and consistency metrics, and rollout diagnostics appropriate to each claim. Action-conditioned adaptation additionally includes a no-action control. Every subsection reports protected-coordinate regressions rather than hiding them in an average.

C.2 Complete ACWM-Phys Repair Results

Table 15 provides the complete eight-environment result behind the main-text summary. Deltas are computed as repair minus baseline under the frozen ACWM-Phys evaluator. Positive PSNR and SSIM and negative masked MSE are favorable. The evidence column distinguishes single-checkpoint passes from repeated formal receipts with stronger claim support.

Table 15: **Failure-specific repair on all eight ACWM-Phys environments.** The selected repair differs across diagnosed failure families; status records the available confirmation boundary.

Environment	Failure family	Selected repair	Checkpoint/evidence
push_cube	rigid contact/action	cfg schedule $1 \to 1.1$	2 receipts
stack_cube	support/contact	cfg schedule $1 \to 1.5$	2 receipts
push_rope	topology/contact	self-forcing finetune	1 checkpoint
cloth_move	deformable memory	next forcing	800 steps
push_sand	granular transport	mixture reweight + scale 0.5	3 receipts
pour_water	fluid transport	event window + scale 0.25	metric pass
robot_arm	articulated dynamics	self-forcing finetune	800 steps
reacher	target-conditioned control	next forcing + scale 0.02	2 receipts

Environment	ΔPSNR $\uparrow$	ΔSSIM $\uparrow$	ΔmMSE $\downarrow$	Status
push_cube	+0.15	+0.0002	-0.000284	formal
stack_cube	+0.03	+0.0020	-0.000531	formal
push_rope	+0.02	+0.0008	-0.000151	formal
cloth_move	+0.94	+0.0099	-0.009040	formal
push_sand	+0.64	+0.0010	-0.000783	formal
pour_water	+0.85	+0.0019	-0.001718	formal
robot_arm	+1.08	+0.0098	-0.002230	formal
reacher	+0.06	+0.0002	-0.000119	formal

Table 16: **Ctrl-World results on WorldArena.** The baseline and repaired model use matched data and training schedules; measured compute is reported separately.

Metric	Ctrl-World	VerdiWM
Semantic Alignment $\uparrow$	90.70	**91.30**
Depth Accuracy $\uparrow$	93.28	**96.16**
Aesthetic Quality $\uparrow$	32.75	**36.12**
Background Consistency $\uparrow$	**86.37**	85.11
Dynamic Degree $\uparrow$	**45.32**	43.78
Flow Score $\uparrow$	26.54	**30.35**
Motion Smoothness $\uparrow$	68.75	**81.53**
Subject Consistency $\uparrow$	**84.31**	83.35

C.3 Physical Consistency in Ctrl-World

The original Ctrl-World produces plausible short-term predictions but exhibits motion drift, object-state jumps, and unstable long-horizon transitions. Its diagnostic response suggests that the failure is concentrated in latent state evolution rather than the visual encoder or renderer. VerdiWM therefore adds a LaMo-style branch containing a motion prior, delta-latent predictor, and drift readout. The objective combines reconstruction and drift consistency,

$$L_{\text{total}} = L_{\text{MSE}} + \lambda_{\text{drift}} L_{\text{drift}}, \tag{20}$$

where L_{drift} aligns the predicted latent displacement with the future motion direction.

Motion smoothness increases from 68.75 to 81.53, while SSIM, LPIPS, and FID also improve. The effect is not uniformly favorable: background consistency drops by 1.26, dynamic degree by 1.54, subject consistency by 0.96, and PSNR is approximately flat. Under the frozen validity gate, the first and third changes remain within tolerance, while dynamic degree exceeds tolerance on the open-drawer context group. The confirmed claim is therefore restricted to contexts whose protected gates pass, with the dynamic-degree regression stored as a boundary annotation.

Table 17: **Ctrl-World video quality.** Lower is better for LPIPS and FID.

Metric	Ctrl-World	VerdiWM
PSNR ↑	**20.5099**	20.4921
SSIM ↑	0.7799	**0.7899**
LPIPS ↓	0.1528	**0.1432**
FID ↓	54.0076	**51.7057**

Table 18: **Cosmos-Predict 2 results on WorldArena.** Baseline versus REP-guided repair under matched training schedules; measured compute is reported separately.

Metric	Cosmos-Predict 2	VerdiWM
Semantic Alignment ↑	90.38	**90.82**
Depth Accuracy ↑	95.35	**97.05**
Aesthetic Quality ↑	36.05	**37.30**
Background Consistency ↑	**85.35**	82.73
Dynamic Degree ↑	42.18	**43.15**
Flow Score ↑	29.55	**30.70**
Motion Smoothness ↑	78.93	**81.31**
Subject Consistency ↑	**83.07**	81.79

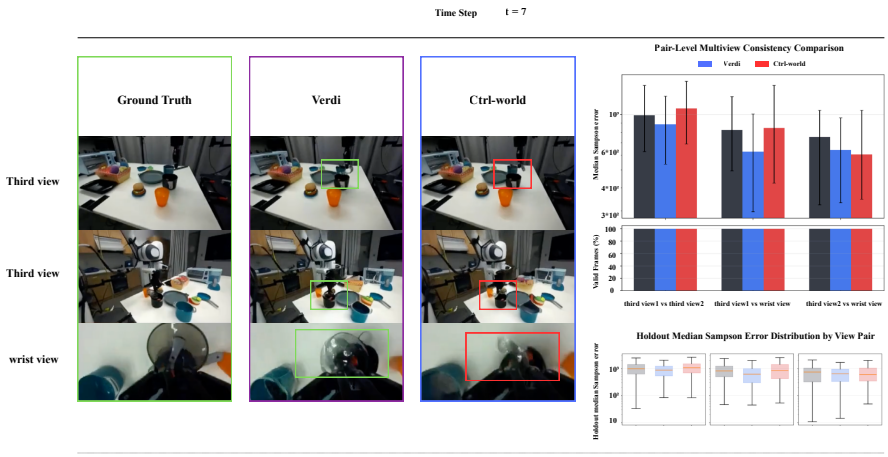


Figure 7: Consistency comparison across three camera views on the "put the lid on" task (DROID (Khazatsky et al., 2024)). Two views improve significantly over the Ctrl-World baseline; third-person view 2 and the wrist view degrade, consistent with the validity-gate analysis above.

C.4 Structure and Long-Horizon Generation in the Cosmos Family

The Cosmos family exposes two different failure modes. Cosmos-Predict 2 shows structural drift under complex motion and occlusion, whereas Cosmos3 shows train–inference mismatch and compounding error during long rollouts. VerdiWM therefore selects representation guidance for the former and self-forcing for the latter rather than applying one global recipe.

Cosmos-Predict 2: representation-guided prediction. REP injects DINO features as an additional constraint so that prediction is aligned not only in pixel space but also in a higher-level structural feature space. Table 18 reports improvements in semantic alignment, depth, flow, and motion smoothness.

Background consistency drops by 2.62 and subject consistency by 1.28. The background regression exceeds its tolerance on the BridgeData V2 (Walke et al., 2023) context group, so the retained claim is restricted to structural coordinates and the static-background failure is recorded as a boundary of the REP entry.

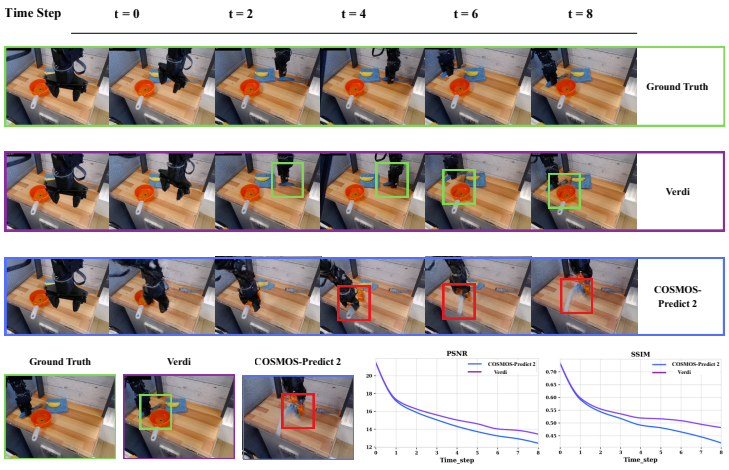


Figure 8: Qualitative comparison of Cosmos-Predict 2 vs. REP on "place the fork in the pot" (BridgeData): ground truth, baseline, and REP-improved prediction.

Cosmos3: self-forcing. Cosmos3 performs well in short rollouts but accumulates subject and background drift as generated states become its own context. Self-forcing exposes the model to generated histories during training while preserving its architecture and input–output interface. This directly targets the diagnosed train–inference mismatch.

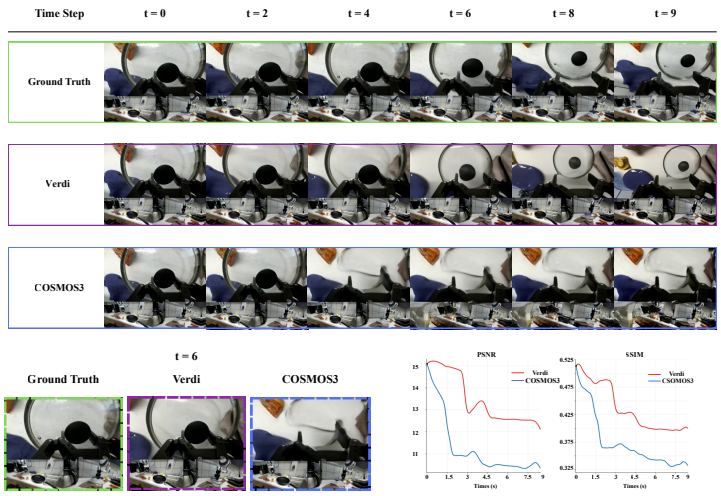


Figure 9: Long-horizon generation on "loosen the pot handle" (DROID (Khazatsky et al., 2024)): COSMOS3 baseline vs. self-forcing. The baseline accumulates subject drift and background instability; self-forcing maintains visual stability and temporal consistency.

C.5 From Video Quality to Action Quality

We test whether the Cosmos3 repair also improves action generation. Vanilla and repaired Cosmos3 act as closed-loop action generators in Franka simulation and real-robot settings. Simulation covers pick-and-place, drawer opening, and peg insertion with 50 trials per arm and task; the real robot covers the first two tasks with 20 trials per arm and task. Both use eight-step action chunks with re-observation after each chunk.

The repaired model improves average simulation success by 18.0 percentage points and average real-robot success by 17.5 points. The effect increases with task horizon, consistent with a repair

Table 19: **Closed-loop manipulation success rate.** Point estimates from paired simulation initial states and real-robot trials. Δ is in percentage points.

Environment	Task	Avg. steps	Vanilla Cosmos3	Repaired	Δ
Sim (n=50)	Pick-and-place	8	62%	**74%**	+12.0
Sim (n=50)	Drawer opening	11	41%	**59%**	+18.0
Sim (n=50)	Peg insertion	14	28%	**52%**	+24.0
Real (n=20)	Pick-and-place	8	55%	**70%**	+15.0
Real (n=20)	Drawer opening	11	35%	**55%**	+20.0

Table 20: **Action-level metrics.** Expert-action L2 error and success decay between the 8-step and 14-step tasks.

Metric	Vanilla Cosmos3	Repaired
Expert-action L2 error ↓	0.084	**0.061**
Success decay ↓	−34 pts	**−22** pts

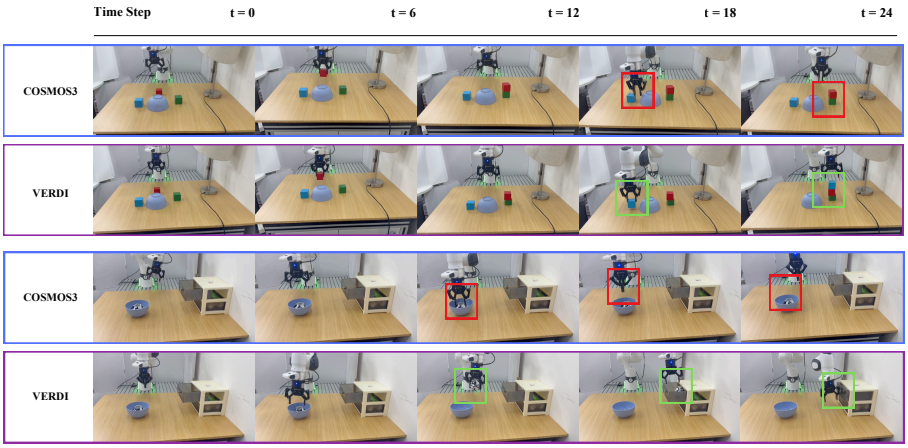


Figure 10: **Real-robot head-to-head rollouts** (Franka Panda, two tasks, sampled at t=0, 6, 12, 18, 24). Top pair: pick-and-place; bottom pair: object into drawer. In each pair, the vanilla Cosmos3 arm (blue border) drifts in late stages and fails (red boxes: grasp/object misplacement), while the repaired arm (purple border) maintains consistent progress and completes the task (green boxes). Identical initial states and instructions across arms.

that targets compounding rollout error. Expert-action L2 error decreases from 0.084 to 0.061, while long-horizon success decay narrows from 34 to 22 points.

C.6 Automatic Adaptation to RoboCoin

RoboCoin tests a different capability: converting a dataset with a new robot embodiment, action interface, camera layout, and task distribution into an executable world-model training task. VerdiWM parses episode boundaries, observations, action sequences, camera identities, temporal alignment, and embodiment metadata, then constructs a unified training and replay contract. It selects the DreamDojo/Cosmos-Predict 2.5 action-conditioned model initialized from AgiBot post-training weights and materializes the field mapping, action-conditioning, temporal sampling, and camera organization.

For single-view adaptation, the video stream is aligned with robot actions to form an action-conditioned future-video prediction task. The no-action control tests whether the prediction actually depends on the action input. Action conditioning improves held-out LPIPS by 0.029 and SSIM by 0.039 relative to this control. For multi-view adaptation, synchronized camera identities are retained

rather than treating views as interchangeable; the reported cross-view subject-consistency variance is 0.029 versus 0.083 for independent per-view adaptation.

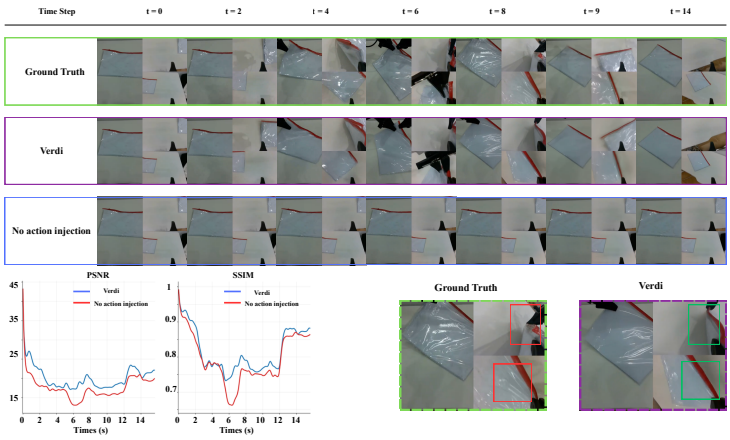


Figure 11: Action-conditioned adaptation on RoboCoin ("opening the red folder"): ground-truth future, action-conditioned prediction, and no-action control, organized in the same camera order and time frame across all three synchronized views. The gap between the action-conditioned and no-action rows evidences that the model uses the action input rather than unconditional visual continuation.



Figure 12: **Ground-truth vs. predicted frames on two RoboCoin tasks** (box relocation, top pair; cup pouring, bottom pair; two synchronized views per time step). VerdiWM-adapted Cosmos-Predict 2.5 (purple) tracks the ground truth (green) closely on both tasks, including object identity and multi-view correspondence.

This experiment establishes a working adaptation contract for one dataset family and one base model. It does not by itself establish adaptation to arbitrary embodiments or datasets.

C.7 Qualitative Visualizations

The remaining qualitative visualizations are retained in the supplementary material.

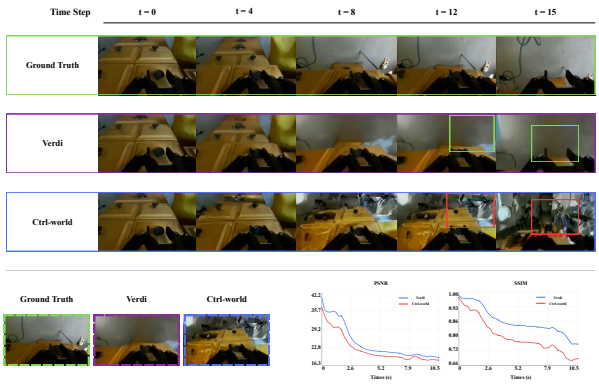


Figure 13: Qualitative comparison on the wrist-camera view of the "open drawer" task (DROID (Khazatsky et al., 2024)): ground-truth future, Ctrl-World baseline, and the VerdiWM-improved model. The baseline tends to replicate the current frame's appearance; the improved model produces explicit action-related changes with higher motion smoothness.

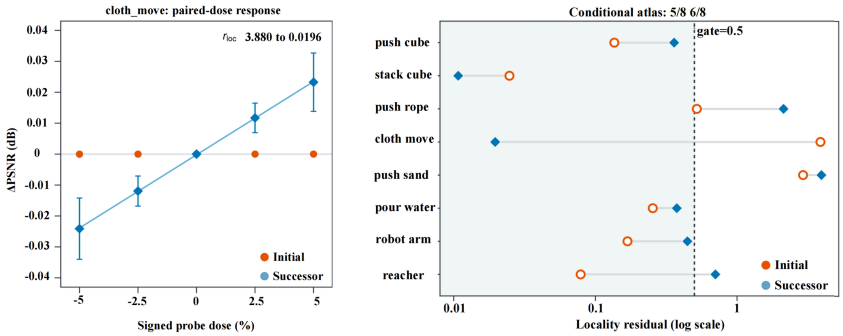


Figure 14: **Counterexample-driven probe evolution.** A non-local response triggers a typed temporal-mix probe. The library keeps both charts and admits the successor only where its paired-dose locality gate passes.